Synaptotagmin IV Modulation of Vesicle Size and Fusion Pores in PC12 Cells

Zhenjie Zhang, Zhen Zhang, and Meyer B. Jackson*
Department of Physiology, University of Wisconsin-Madison, Madison, Wisconsin

ABSTRACT Many synaptotagmins are Ca^{2+}-binding membrane proteins with functions in Ca^{2+}-triggered exocytosis. Synaptotagmin IV (syt IV) has no Ca^{2+} binding activity, but nevertheless modulates exocytosis. Here, cell-attached capacitance recording was used to study single vesicle fusion and fission in control and syt IV overexpressing PC12 cells. Unitary capacitance steps varied widely in size, indicating that both microvesicles (MVs) and dense-core vesicles (DCVs) undergo fusion. Syt IV overexpression reduced the size of DCVs and endocytotic vesicles but not MVs. Syt IV also reduced the basal rate of Ca^{2+}-induced fusion. During kiss-and-run, syt IV increased the conductance and duration of DCV fusion pores but not MV fusion pores. During full-fusion of DCVs syt IV increased the fusion pore conductance but not the duration. Syt IV overexpression increased the duration but not the conductance of fission pores during endocytosis. The effects of syt IV on fusion pores in PC12 cells resembled the effects on fusion pores in peptidergic nerve terminals. However, differences between these and results obtained with amperometry may indicate that amperometry and capacitance detect the fusion of different populations of vesicles. The effects of syt IV on fusion pores are discussed in terms of structural models and kinetic mechanisms.

INTRODUCTION

Many synaptotagmins are Ca^{2+}-binding proteins that function in regulated exocytosis. Synaptotagmin IV (syt IV) has no known Ca^{2+} binding activity (1–4), but nevertheless modulates exocytosis of large dense-core vesicles (DCVs) and small clear microvesicles (MVs) in peptidergic nerve terminals (5). Syt IV has a number of effects on fusion pores. In mice lacking syt IV, fusion pores during transient DCV kiss-and-run events are smaller than in wild-type, but fusion pores during MV kiss-and-run events are indistinguishable from wild-type (5). In *Drosophila* motor nerve terminals the presence of syt IV alters the time course of unitary release events in a manner consistent with alterations in fusion pore dynamics (6). In hippocampal neurons, presynaptic syt IV changed the amplitude of miniature synaptic currents (7). Amperometry recording in PC12 cells showed that syt IV altered fusion pore duration without changing pore size (8,9). Because the fusion pore is an important kinetic intermediate of membrane fusion, these effects of syt IV may be relevant to the mechanism of exocytosis. Furthermore, fusion pores are thought to influence the time course of synaptic transmitter release (10–12), and can selectively filter substances that are released from a vesicle (13). Thus, effects on fusion pores have implications for biological function.

Among the various studies of fusion pores just surveyed, the capacitance results showing that syt IV alters fusion pore size in peptidergic nerve terminals (5) seem to be in conflict with amperometry results showing that syt IV overexpression primarily alters fusion pore kinetics (8,9). In these studies syt IV overexpression did not alter pore size but favored a kiss-and-run mode of release that uses a smaller fusion pore. Because these studies differ in both biophysical method and biological preparation, the origin of the discrepancy remains unclear. Whereas capacitance recording monitors the conductance of fusion pores, amperometry detects the efflux of readily oxidized chemicals such as norepinephrine. Capacitance can detect the fusion of MVs, even when they contain no readily oxidized substance. To obtain data from PC12 cells that can be compared more directly with the data from peptidergic nerve terminals, we have used capacitance recording to study fusion pores in PC12 cells. PC12 cells express very low levels of endogenous syt IV, and transfection with cDNA encoding syt IV increases the expression of this protein (14). We report that, as in peptidergic nerve terminals, in PC12 cells syt IV overexpression increases the conductance of fusion pores during DCV fusion, but not during MV fusion. Furthermore, in parallel with amperometry data from PC12 cells, capacitance recording showed kiss-and-run events with longer lifetimes in syt IV overexpressing cells compared to control cells. Full-fusion pores changed their size but not their kinetics whereas endocytotic fission pores increased their duration but showed no significant change in size. These results show that syt IV can influence trafficking at the plasma membrane in a wide variety of ways.

METHODS

Molecular biology

Syt IV was subcloned into the pIRES2EGFP vector (Clontech, Mountain View, CA) with the restriction sites *Nhe*1 and *Sma*1 (9). This construct

Submitted August 12, 2009, and accepted for publication November 18, 2009.

*Correspondence: mjackson@physiology.wisc.edu

Zhenjie Zhang's present address is Department of Molecular and Cell Biology, University of California, Berkeley, CA.

Editor: Francisco Bezanilla.

© 2010 by the Biophysical Society
0006-3495/10/03/0968/11 $2.00

doi: 10.1016/j.bpj.2009.11.024

expresses enhanced green fluorescent protein (EGFP) from an internal ribosome entry site and syt IV from the encephalomyocarditis virus promoter. This arrangement permits identification of transfected cells in a fluorescence microscope.

Cell culture and DNA transfection

PC12 cells from passage number 30–50 were cultured in 100 mm diameter dishes in Dulbecco's modified Eagle's medium at 37°C in a humidified atmosphere of 5% CO_2–air. Dulbecco's modified Eagle's medium was supplemented with 4.5 mg/ml glucose, 3.7 mg/ml $NaHCO_3$, 5% equine serum, and 5% iron-supplemented bovine calf serum (15). For recordings, cells were transferred to coverslips freshly coated with collagen-I (BD Bioscience, Bedford, MA) and poly-D-lysine (Sigma-Aldrich, St. Louis, MO) in 24-well plates.

DNA transfection was carried out in an ECM-830 electroporator (BTX, San Diego, CA) with a 210 V, 7 ms voltage pulse. Transfection was carried out on cells suspended in a solution consisting of (in mM): 120 KCl, 0.15 $CaCl_2$, 10 KH_2PO_4, 2 EGTA, 5 $MgCl_2$, 2 Mg-ATP, 5 glutathione, and 2.5 HEPES (pH 7.6) containing 50–100 μg DNA. Recordings were made 36–96 h after transfection. PC12 cells transfected with a blank pIRES2EGFP vector were used as controls.

Western blot and protein purification

Syt I C2AB or syt IV C2AB bearing GST tags were grown in *Escherichia coli* at 37°C to an OD_{600} of 0.8, induced by addition of 0.4 mM IPTG for 4 h, pelleted, resuspended in HBS (100 mM NaCl and 25 mM HEPES, 1 mM DTT, pH 7.4), sonicated, and treated with Triton X-100 and protease inhibitors. The supernatant was collected after centrifugation and incubated with rotation overnight with glutathione-Sepharose beads at 4°C. Beads were washed 2× with wash buffer (1 M NaCl and 25 mM HEPES, pH 7.4) and 2× with HBS + 0.1 mg/mL RNase and DNase. Bound protein was eluted by boiling in SDS buffer. Protein concentration was determined by SDS-PAGE and Coomassie blue staining against a *bovine serum albumin* standard curve.

For Western blots PC12 cells were harvested in PBS with 1% Triton X-100 and 5 mM PMSF, incubated at 4°C for 30 min, and centrifuged at 21,000 × *g* for 10 min. Supernatants were transferred to new tubes and protein concentration was determined using the BCA protein assay kit (Pierce Chemical, Rockford, IL). Protein extracts (10 μg) and designated amount of protein standard were subjected to SDS-PAGE. Proteins were detected with monoclonal antibodies against syt I (Cl 41.1) and syt IV (Synaptic Systems, Göttingen, Germany), followed by secondary horse radish peroxidase conjugated antibody, and developed with enhanced chemiluminescence (Pierce Chemical).

Western blots show the expression levels of syt I and syt IV in control and syt IV overexpressing cells (Fig. 1). With reference to standards, the amount of syt IV in transfected PC12 cells increased ~2.5-fold. Because only 20% of the cells were transfected (based on counting cells expressing EGFP), we estimate that the expression level in transfected cells increased ~12.5-fold. However, even with syt IV overexpression, syt IV levels were only ~10% of endogenous syt I. Overexpressing syt IV produced no change in syt I levels.

Capacitance recording

The recording of capacitance from cell-attached patches follows methods published previously (16,17). Cells attached to coverslips were bathed in a recording solution consisting of (in mM): 125 NaCl, 4 KCl (40 mM for syt IV cell experiments), 10 $CaCl_2$, 2 $MgCl_2$, 10 HEPES, pH 7.3. The patch pipette solution for cell-attached patch recording was the same but contained 15 mM TEA and 3 μM tetrodotoxin. To reduce the noise, patch pipettes were pulled from thick wall borosilicate glass capillaries (OD = 1.5 mm or 1.7 mm, ID = 0.85 mm; Garner Glass, Claremont, CA), and were heavily coated with Sylgard (Sylgard 184 kit; Dow Corning, Midland, MI). To reduce noise further pipettes were filled with the minimum amount of solution that allowed electric contact with the AgCl wire.

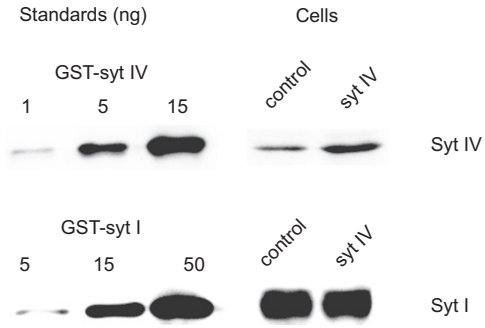

FIGURE 1 Western blot showing expression of syt IV (*above*) and syt I (*below*). Expression in PC12 cells is shown on the right; standards with recombinant protein are on the left. The syt IV signal was ~2.5 times higher in syt IV overexpressing than control cells. Accounting for the fraction of cells transfected gives 12.5-fold higher syt IV levels in transfected cells. Syt I levels were indistinguishable in control and syt IV overexpressing cells.

Sine waves of 20 kHz and 100–200 mV root mean-square were generated by the lock-in amplifier (SR830; Stanford Research, Synnvale, CA) and superimposed on a holding-potential of 0 mV. The patch clamp (EPC-7; Instrutech, Port Washington, NY), output was fed into the lock-in amplifier through a 5:1 voltage divider. Outputs of the lock-in amplifier were low-pass filtered at 3 ms. The patch-clamp amplifier gain was set at 50–100 mV/pA, the C_{slow} potentiometer was set at the minimum value, the G_{slow} potentiometer was set at 0.2 μS, and the C_{fast} and τ_{fast} potentiometers were adjusted to cancel out the sinusoidal current.

The phase setting of the lock-in amplifier was adjusted to eliminate signals in the real (Re) trace while dithering a 100 fF capacitance step built into the capacitance compensation circuit. Membrane capacitance changes were subsequently calibrated with a pulse to the capacitance compensation circuitry to produce a 1 fF step in the imaginary (Im) trace. Gentle suction was occasionally applied to the pipette to check the phase setting, by checking whether the membrane extension resulted in an increase only in the Im signal. An additional phase adjustment was carried out offline recalculating the Re and Im traces with 2° phase increments to eliminate the projection of full exocytosis steps from the Im signal to the Re signal (18). Capacitance steps were identified as instantaneous jumps of more than twice the RMS noise to a stable new level.

Fusion pore conductance was calculated from the Re and Im traces with the following equation (16,19):

$$G_p = \left(\mathrm{Im}^2 + \mathrm{Re}^2\right)/\mathrm{Re}. \quad (1)$$

By considering the fusion pore as a simple cylindrical resistor filled with a medium with a resistivity of 100 Ωcm (that of saline, ρ) and a pore length, λ, of 15 nm (that of a gap junction), we estimated the pore radius with the following equation (20):

$$r_p = \left(G_p \rho \lambda/\pi\right)^{1/2}. \quad (2)$$

Cells were depolarized by puffing a solution containing (mM) 130 KCl, 10 NaCl, 10 $CaCl_2$, 2 $MgCl_2$, and 10 HEPES (pH 7.3) from a micropipette 10–20 μm away. Solution was ejected with pressure from a Picospritzer (Parker-Hannefin, Cleveland, OH).

RESULTS

Spontaneous fusion and fission steps

Cell-attached patch recordings from PC12 cells showed unitary stepwise changes as individual vesicles fused with

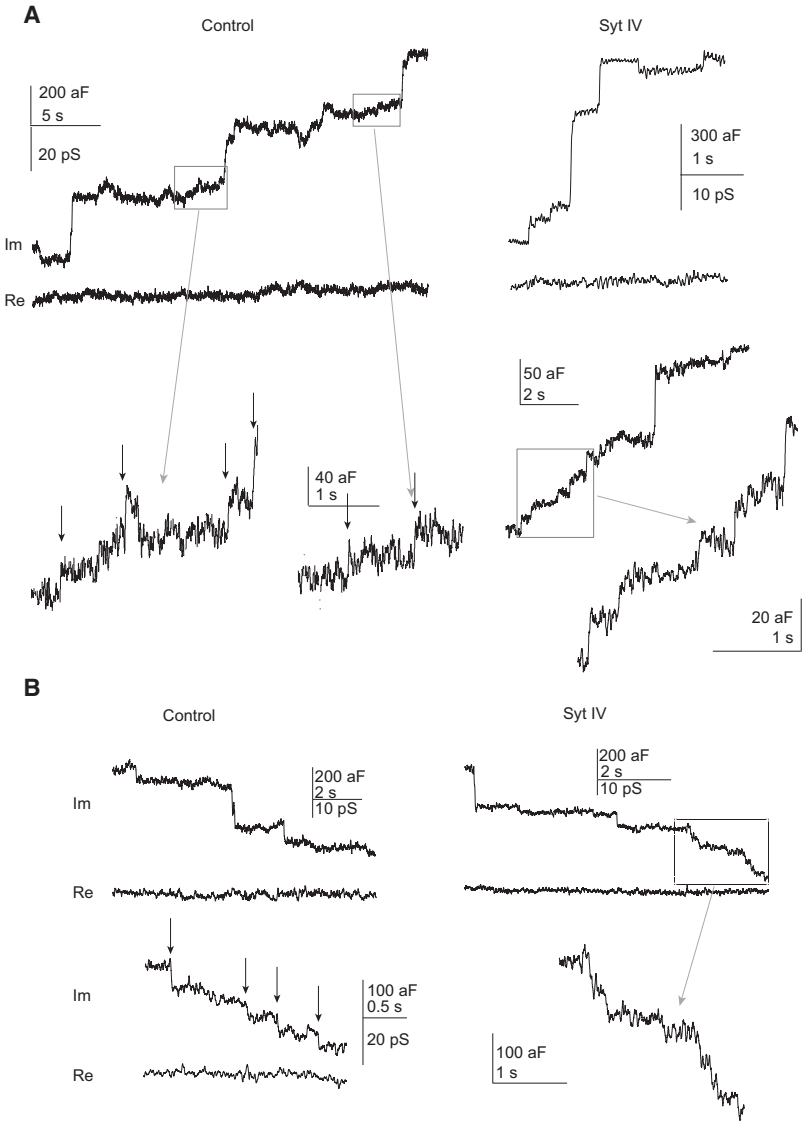

FIGURE 2 Single vesicle capacitance steps in PC12 cells. (*A*) Upward steps signal the exocytosis of both single DCVs (*upper panels*) and single MVs (*lower panels*) in control (*left*) and syt IV overexpressing (*right*) PC12 cells. Areas in boxes were expanded to show small steps clearly. (*B*) Downward steps signal the endocytosis of vesicles of varying size in control and syt IV PC12 cells.

the plasma membrane. These recordings contain information about vesicle size and fusion frequency as well as about fusion pores. We first present our results on vesicle size and fusion frequency before turning to fusion pores.

PC12 cells contain both synaptic vesicle-like microvesicles (MVs) and dense-core vesicles (DCVs) (21). These two types of vesicles have very different sizes, and because vesicle membrane area is proportional to capacitance, capacitance recording can detect and distinguish between the MVs from DCVs. Capacitance recordings from both control PC12 cells (transfected with control vector) and cells overexpressing syt IV showed upward (Fig. 2 *A*) and downward (Fig. 2 *B*) capacitance steps. The steps occurred spontaneously in control cells in normal bathing solution, but in cells overexpressing syt IV spontaneous steps were extremely rare. For this reason extracellular KCl was raised to 40 mM in experiments with syt IV cells. This resulted in a moderate depolarization to increase the frequency of capacitance steps to a level comparable to that in control cells. Capacitance step frequency will be discussed further below.

Capacitance steps in cell-attached patches had a broad range of amplitudes. For both DCVs and MVs, the size distributions were similar between control cells and cells overexpressing syt IV (Fig. 3 *A*). Based on the known sizes of MVs and DCVs we estimated that 80 aF would serve as a useful cutoff to distinguish between them. The events below 80 aF were taken as MVs and their sizes were similar in control and syt IV cells (control: 45.7 $\pm$ 0.9 aF, $n = 318$; syt IV: 45.7 $\pm$ 0.5 aF, $n = 1104$; $p = 0.49$). By contrast, DCVs (capacitances $>$ 80 aF) were significantly smaller in syt IV cells (control: 256 $\pm$ 24 aF, $n = 235$; syt IV: 195 $\pm$ 8 aF, $n = 777$; $p = 0.003$) (Fig. 3 *B*). We converted capacitance to vesicle membrane area assuming spherical geometry and taking the specific membrane capacitance as 0.9 μF/cm^2 (22). From this conversion we obtained diameters of 39.6 $\pm$ 0.4 nm for control MVs, 39.4 $\pm$ 0.2 nm

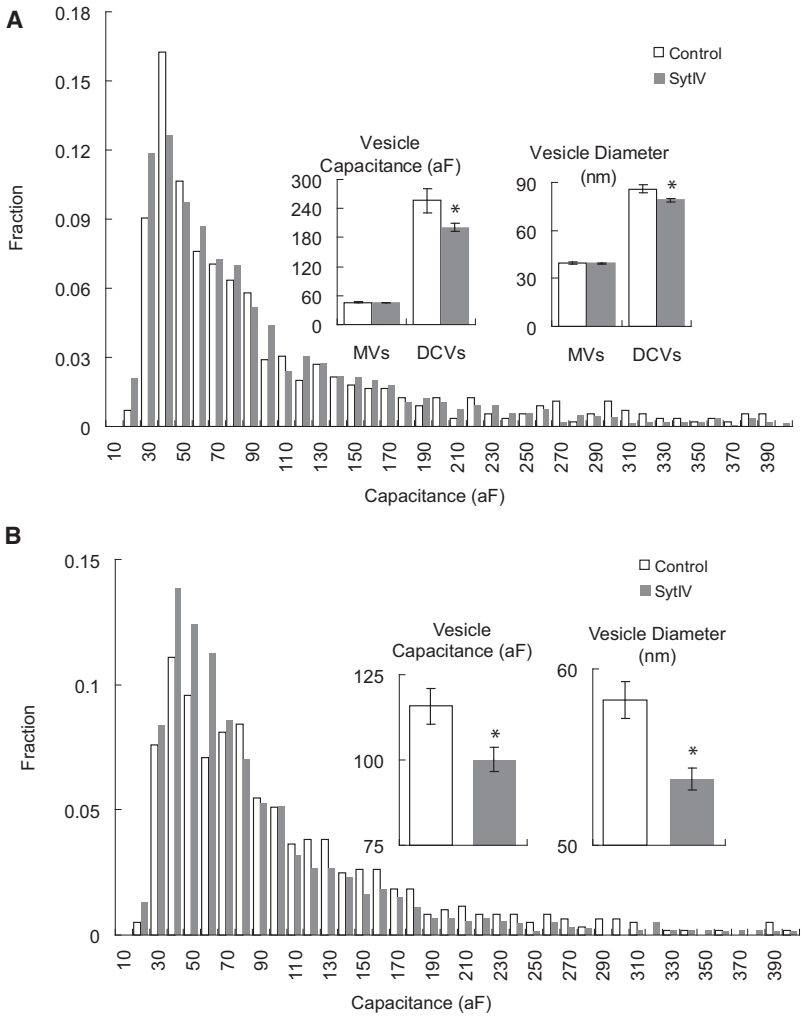

FIGURE 3 Exocytosis and endocytosis step size distributions. (*A*) Exocytosis vesicle size distributions were similar between control (528 total) and syt IV cells (1721 total). Vesicle numbers for each bin were normalized to the total number to obtain fractions. (*Inset*) Average vesicle capacitance (*left*) and diameter (*right*; converted from vesicle capacitance). Stars indicate statistical significance ($p < 0.05$). (*B*) Endocytosis vesicle size distribution for 605 steps from control cells and 1567 steps from syt IV cells. (*Inset*) Average capacitance (*left*) and diameter (*right*).

for syt IV MVs ($p = 0.32$), 86.0 ± 2.7 nm for control DCVs, and 78.0 ± 1.0 nm for syt IV DCVs ($p = 0.002$). Again, the average MV diameters were indistinguishable, but the average DCV diameters were smaller in syt IV overexpressing cells.

Capacitance recordings also contained downward steps (Fig. 2 *B*), which reflect the endocytosis of single vesicles. The size distributions of these steps from control and syt IV cells both have peaks at 40–50 aF, but syt IV overexpressing cells had a larger fraction of smaller endocytotic events (Fig. 3 *B*). The average size of endocytosis steps was significantly larger for control cells (115.8 ± 5.2 aF, 58.2 ± 1.0 nm, $n = 605$) than Syt IV cells (100.1 ± 3.1 aF, 53.6 ± 0.6 nm, $n = 1567$; $p < 0.008$) (Fig. 2 *B*, *inset*). In the posterior pituitary nerve terminals there was no difference in endocytosis vesicle size between syt IV knock-out and wild-type nerve terminals (5). The discrepancy may be due to differences in other molecular components responsible for endocytosis between these two very different biological systems, or to developmental compensation in knock-out animals.

Syt IV reduction of depolarization-evoked exocytosis

Depolarization by puffing 130 mM KCl increased the frequency of upward capacitance steps in ~40% of patches in both control and syt IV cells (Fig. 4 *A*). The failure to induce secretion in 60% of the patches could be due to the local scarcity of vesicles or absence of specialized fusion sites in those patches. Because we patched each cell only once it is also possible that the absence of secretion in a patch reflects variable secretion between cells. In the patches that responded to KCl depolarization, the MV secretion rate of control cells increased from 0.022 ± 0.006/s to 0.090 ± 0.010/s (28 patches), and the DCV secretion rate in control cells increased from 0.010 ± 0.002/s to 0.085 ± 0.018/s (23 patches). In syt IV cells the MV secretion rate increased from 0.016 ± 0.004/s to 0.093 ± 0.008/s (49 patches), and the DCV secretion rate increased from 0.005 ± 0.001/s to 0.057 ± 0.010/s (38 patches) (Fig. 4 *B*). Note that a higher initial bathing KCl concentration of 40 mM had to be used in syt IV cell experiments (versus 4 mM KCl for control cells) to achieve a basal release rate comparable to control cells.

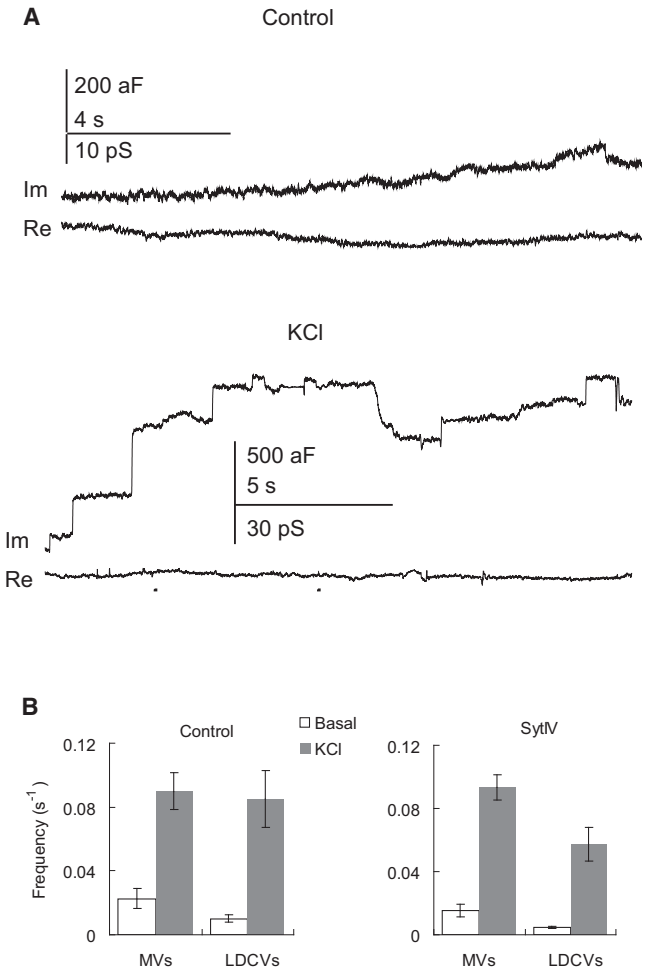

FIGURE 4 KCl depolarization enhanced exocytosis rates in PC12 cells. (*A*) Representative traces of exocytosis at rest (*upper panel*) and with KCl depolarization (*lower panel*). Both are from a control experiment. (*B*) Mean exocytosis rates at resting and depolarized states in control cells (*left*) and syt IV cells (*right*). Higher external KCl (40 mM) was used for "resting" syt IV cells due to the much lower frequency of spontaneous events at 4 mM KCl. Traces were recorded ~5–10 s after applying high KCl (130 mM) to depolarize a cell (see Methods).

Because this means that basal fusion events for control and syt IV cells were measured with different KCl concentrations, we compared the vesicle sizes of each group of cells for the two conditions and found that the bathing KCl concentration had no statistically significant effect (data not shown). Thus, the conditions of rest and depolarization do not alter vesicle size. The lower exocytosis in syt IV overexpressing cells agrees with a previous amperometry study that showed a ~5-fold lower Ca^{2+} sensitivity of DCV release for syt IV cells (8), and is also consistent with the observations of less norepinephrine release from PC12 cells overexpressing syt IV (9). In the posterior pituitary larger whole-terminal capacitance changes were evoked by low Ca^{2+} entry in syt IV knock outs versus wild-type (5).

Kiss-and-run fusion pores

Single-vesicle capacitance traces showed the time course of fusion as exocytosis proceeds through an intermediate fusion-pore state. This fusion pore can either dilate to complete the fusion process (full-fusion), or close to retrieve the intact vesicle (kiss-and-run). Fusion pore closure is a hallmark of kiss-and-run, and is recognized in capacitance recordings as flickers with closely coupled upward and downward steps of similar size (23–26). During these capacitance flickers one can observe simultaneous changes in both the Re and the Im signals of the lock-in amplifier, and these signals can be used to calculate the vesicle capacitance and fusion pore conductance (see Methods).

Amperometry recording has shown that Syt IV regulates kiss-and-run of norepinephrine-containing vesicles in PC12 cells (8). Our capacitance recordings showed kiss-and-run events with sizes in both the MV and DCV ranges (Fig. 5). Of the upward capacitance steps in control cells, 19% of MV steps (61 of 318) and 31% of DCV steps (73 of 235) were followed by downward steps within 3.5 s. The percentages in syt IV cells were nearly the same (16%, 171 of 1055 for MVs and 37%, 280 of 725 for DCVs). The upward and downward steps within each capacitance flicker were closely correlated in size, with linear regression slopes close to one for both (control slope: 0.98 ± 0.01, syt IV slope: 0.98 ± 0.01) (Fig. 5, *C* and *D*, *left*). Pairing upward steps with other downward steps in the same trace or immediately adjacent traces failed to show a statistically significant correlation (Fig. 5, *C* and *D*, *right*). The close correlation of upward and downward steps in kiss-and-run events suggested that there was no lateral diffusion of lipid across the fusion pore. Although this result is consistent with a proteinaceous pore structure, the size of a capacitance flicker could be stable with a lipidic fusion pore provided that the membrane tensions of the vesicle and plasma membranes exactly balance each other (27,28).

Syt IV overexpression significantly increased the conductance of DCV kiss-and-run fusion pores (Fig. 6; control: 119.8 ± 31.4 pS, $n = 47$; syt IV: 224.5 ± 34.5 pS, $n = 110$, $p = 0.03$), but had no significant effect on the conductance of MV kiss-and-run fusion pores (control: 24.0 ± 1.2 pS, n = 9; syt IV: 20.5 ± 3.0 pS, $n = 22$, $p = 0.23$). The fusion pore conductances were indistinguishable between the resting conditions and the KCl depolarizing conditions used to increase the fusion event frequency (data not shown). The fusion pore radius estimated from these conductances with Eq. 2 showed an effect of syt IV on DCVs but not MVs (control DCVs: 0.64 ± 0.06 nm, syt IV DCVs: 0.84 ± 0.06 nm, $p = 0.02$; control MVs: 0.34 ± 0.01 nm, syt IV MVs: 0.30 ± 0.02 nm, $p = 0.12$). A similar result was obtained in peptidergic nerve terminals, where DCV fusion pores in wild-type mouse nerve terminals had nearly twice the conductance of DCV fusion pores compared to syt IV knockouts, whereas MV fusion pore conductances were indistinguishable (5).

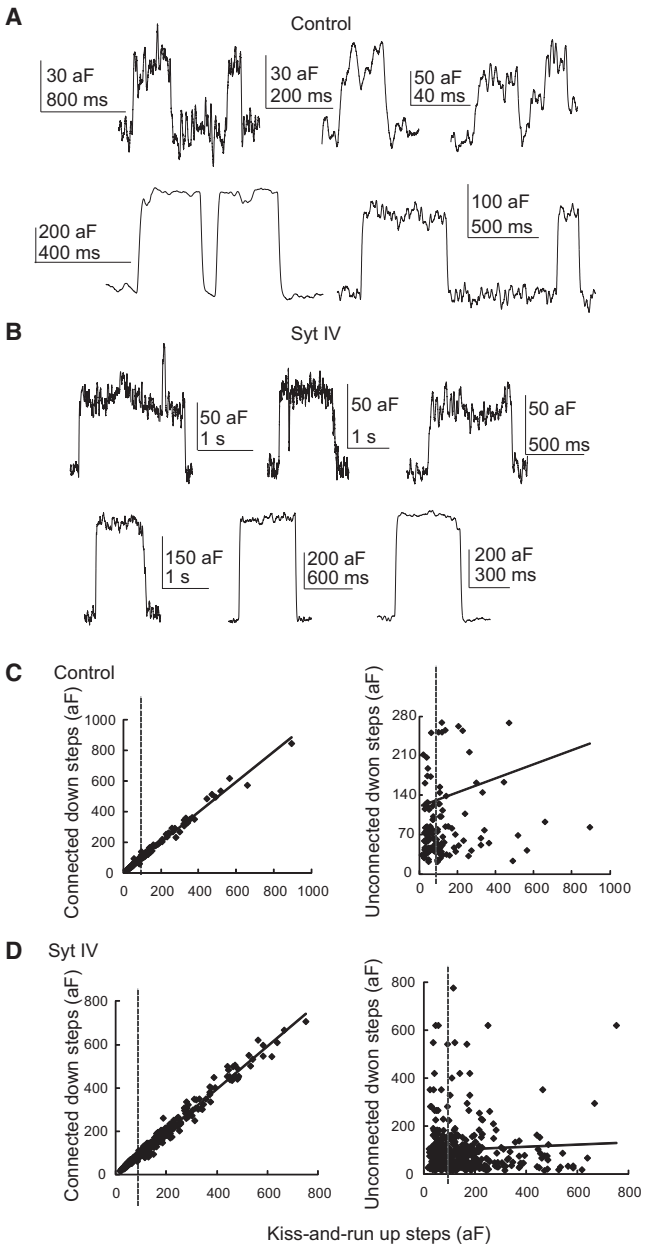

FIGURE 5 Kiss-and-run. (*A*) Representative kiss-and-run events from control cells showing small MV steps (*upper*) and large DCV steps (*lower*). (B) Representative kiss-and-run events from syt IV cells showing MV steps (*upper*) and DCV steps (*lower*). (*C*) Plots of upward and downward steps from kiss-and-run events (*left*) in control cells showed a linear relation with a slope of 0.98. The plot of upward steps in kiss-and-run events versus randomly selected downward steps in the same trace or an immediately adjacent trace showed no correlation. Gray vertical lines denote the position of the 80 aF cutoff used to separate MVs from DCVs. (*D*) The same quantities plotted as in *C* for control cells are shown for syt IV cells. A linear regression slope of 0.98 was found for coupled upward and downward steps, but when downward steps were not paired with the upward step there was no significant correlation.

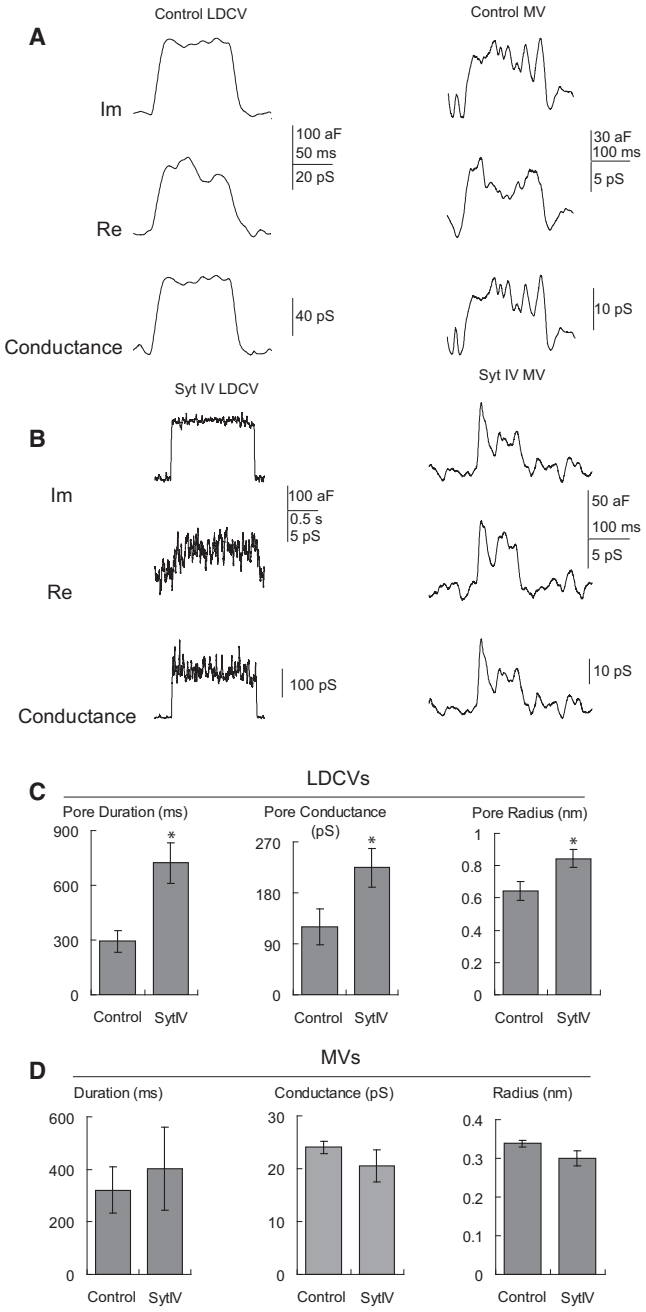

FIGURE 6 Fusion pore reconstruction for kiss-and-run events. The imaginary (Im) and real (Re) lock-in outputs were used to compute conductance traces (see Methods). (*A*) Fusion pore reconstruction in control cells (*left*, DCVs; *right*, MVs). (*B*) Fusion pore reconstructions in syt IV cells (*left*, DCVs; *right*, MVs). (*C*) DCV fusion pore duration (*left*), conductance (*middle*), and radius (*right*) were compared between control and syt IV cells. (*D*) MV fusion pore duration (*left*), conductance (*middle*), and radius (*right*) were compared between control and syt IV cells. Stars indicate statistical significance ($p < 0.05$).

Syt IV overexpression also prolonged DCV kiss-and-run events, increasing their durations from 294 ± 60 ms in control cells to 723 ± 112 ms in syt IV overexpressing cells ($p = 0.008$). MV kiss-and-run events remained unchanged in duration (control: 320 ± 89 ms, syt IV: 402 ± 158 ms, $p = 0.4$). Amperometry recording has also revealed longer lasting kiss-and-run fusion pore durations in syt IV

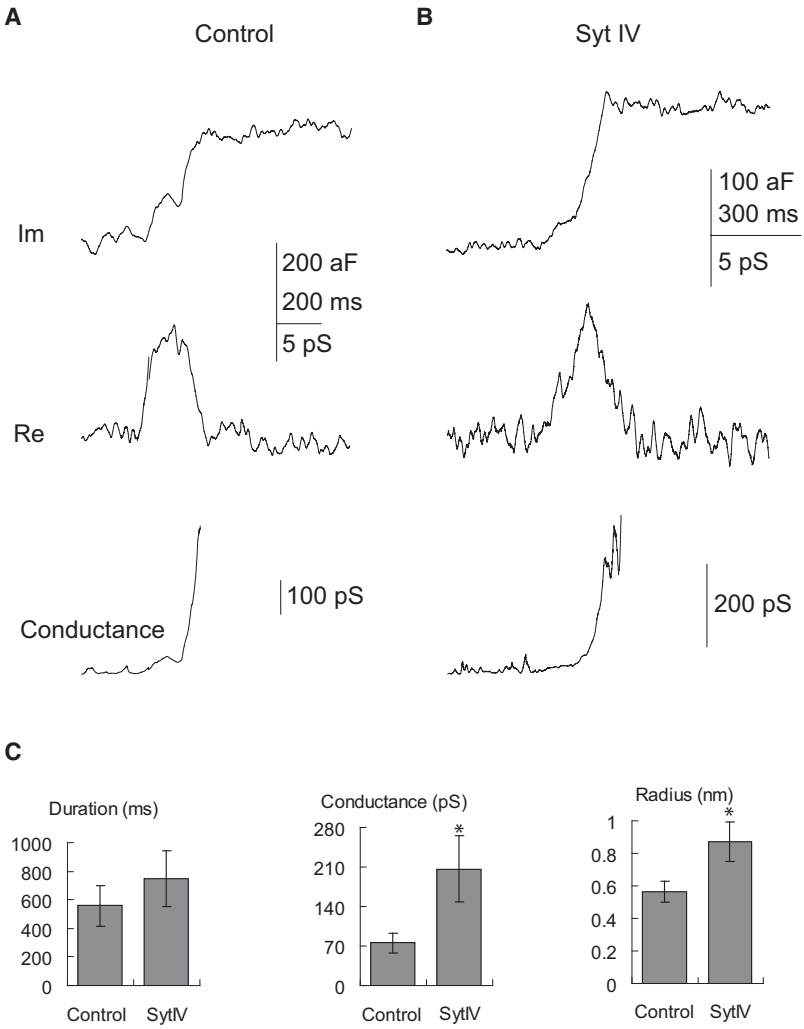

FIGURE 7 Fusion pore reconstruction for full-fusion events, computed from the lock-in outputs as in Fig. 6. (*A*) Pore conductance during full fusion from a control cell. (*B*) Pore conductance during full fusion from a syt IV cell. (*C*) Full fusion pore duration (*left*), conductance (*middle*), and radius (*right*) were compared between control and syt IV cells. Stars indicate statistical significance ($p < 0.05$).

overexpressing PC12 cells (8). However, in wild-type and syt IV knock-out nerve terminals, both DCV (462 ± 167 msec in wild-type and 459 ± 100 msec in syt IV knock-out) and MV (629 ± 127 msec in wild-type and 745 ± 161 msec in syt IV knock-out) kiss-and-run event durations were indistinguishable (Z. Zhang and M. Jackson, unpublished).

Fusion pores during full-fusion

Fusion pores can also be detected in capacitance recordings at the onset of full-fusion events. MV fusion pores were very difficult to detect due to their small size, and possibly due to their brief lifetime (25,26). During full-fusion of DCVs the transient rise in the Re trace of the lock-in amplifier and the delay until the Im trace reaches its final level indicate the formation of a fusion pore (Fig. 7 *A*). Like kiss-and-run fusion pores, fusion pores associated with full-fusion had higher conductances in syt IV cells than in control cells (control: 76 ± 17 pS, $n = 12$, syt IV: 209 ± 59 pS, $n = 15$, $p = 0.04$; control pore radius: 0.56 ± 0.06 nm, syt IV pore radius: 0.87 ± 0.12 nm, $p = 0.03$). Although syt IV overexpression increased the duration of these events, the difference was not statistically significant (control: 558 ± 140 ms, syt IV: 747 ± 198 ms, $p = 0.24$).

Endocytosis and fission pores

Downward steps in capacitance signal the endocytosis of single vesicles, and during these transitions we occasionally detected fission pores (Fig. 8). We found that syt IV overexpression did not significantly alter fission pore conductance (control: 214 ± 73 pS, n = 13, syt IV: 168 ± 50 pS, $n = 20$, $p = 0.30$) or the inferred radius (control: 0.89 ± 0.14 nm, syt IV: 0.72 ± 0.11 nm, $p = 0.18$). However, syt IV overexpression approximately doubled fission pore duration (control: 294 ± 44 ms, syt IV: 629 ± 160 ms, $p = 0.03$). These results indicate that syt IV participates in fission pore kinetics, and presumably interacts with components of the endocytotic machinery. Note that although the Im trace of Fig. 8 *B* shows two downward steps, this should not be interpreted as the endocytosis of two vesicles. Because the Re trace is also changing, the Im trace is not literally vesicle capacitance. In general, endocytosis events presented fusion

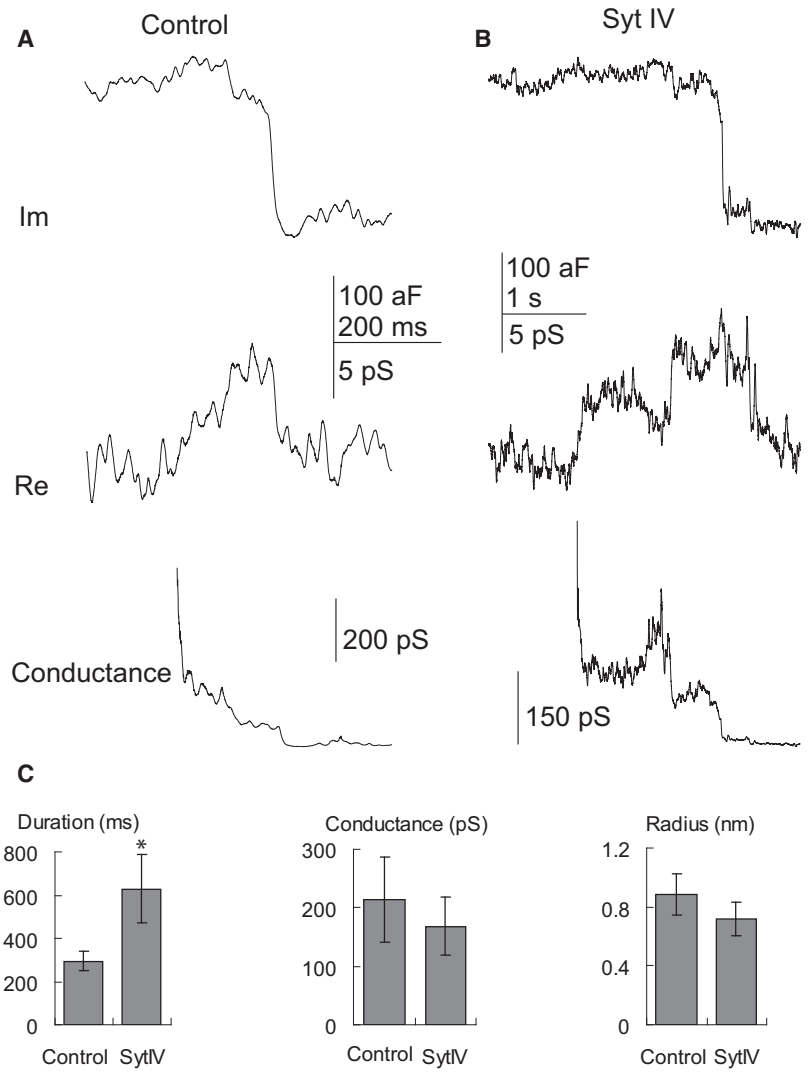

FIGURE 8 Fission pore reconstruction for endocytosis events, computed from the lock-in outputs as in Fig. 6. (*A*) Fission pore reconstruction from a control cell. (*B*) Fission pore reconstruction from a syt IV cell. (*C*) Fission pore duration (*left*), conductance (*middle*), and radius (*right*) were compared between control and syt IV cells. Stars indicate statistical significance ($p < 0.05$).

pores very rarely so the probability of two coincident fission events, both presenting pores, is extremely low.

DISCUSSION

In this study, we have investigated the effects of syt IV on membrane fusion and fission in PC12 cells. Using measurements of complex impedance in cell-attached patches of membrane we determined vesicle capacitance and fusion pore properties in control cells and cells with ~10-fold higher syt IV (Fig. 1). Information at this level of detail offers insights into the role of syt IV, and the mechanisms by which this protein regulates exocytosis and endocytosis. The comparison between cells transfected with control vector and cells transfected with vector harboring the sequence encoding syt IV provides two systems that differ primarily in the abundance of syt IV. However, although syt I levels remain the same (Fig. 1), unintended perturbations of other proteins cannot be excluded. Amperometry studies have indicated that transfection with various syt isoforms and mutants have specific effects on the exocytosis machinery (3,8,9,29). Here we explored effects of one syt isoform in much greater detail with a more powerful technique. Considering that syt IV levels remained well below syt I levels even after syt IV overexpression (Fig. 1), it is unlikely that the changes in vesicles and fusion pores reflect a nonspecific effect of overexpression but this possibility cannot be rigorously excluded.

Changes in vesicle size

Capacitance recording showed that syt IV overexpression reduced the size of fusing DCVs but not MVs, and amperometry has revealed a small insignificant decrease in DCV norepinephrine content (9). Electron microscopy showed that syt IV was present on larger DCVs in PC12 cells (8), and was enriched in larger immature secretory granules of ATT-20 cells (30). Given that syt IV inhibits exocytosis, its presence on larger DCVs will lead to their accumulation whereas smaller DCVs will fuse and produce smaller capacitance steps.

In mouse posterior pituitary nerve terminals genetic ablation of syt IV increased DCV diameter in the electron microscope but produced a small and statistically insignificant reduction in DCV capacitance (5). The different results in this genetic model may indicate that compensatory mechanisms are triggered in an organism by the loss of syt IV. It is also possible that the actions of syt IV depend on interactions with other proteins so that its effects are context dependent. The different kinetic profiles of single vesicle fusion events of syt IV harboring vesicles in the dendrites and axons of hippocampal neurons may be another example of context specific effects (7).

Variations in fusion pore size

Syt IV overexpression produced an approximate doubling of DCV fusion pore conductance during both kiss-and-run (Fig. 6 *C*) and full-fusion (Fig. 7 *C*). This effect was specific for DCVs; MV fusion pores were not affected. The presence of syt IV has a similar effect in pituitary nerve terminals. Nerve terminals from syt IV knock-out animals had DCV fusion pore conductances of about half that seen in wild-type and no difference could be detected between MV fusion pores from the two animals (5). Amperometry recordings from PC12 cells also showed that syt IV overexpression altered fusion pores (8), but in a way that is difficult to reconcile with this capacitance data. Amperometry showed that syt IV overexpression increased the frequency of events through a mode that was exclusively kiss-and-run. This mode used a fusion pore that had a ~5-fold lower flux of norepinephrine than the fusion pores that can lead to full fusion. The amperometric fusion pores that lead to full fusion appear as prespike feet that last only 1–2 ms, a duration too brief to detect with capacitance. By contrast, the small amplitude kiss-and-run fusion pores have longer lifetimes of ~20–80 ms, depending on whether syt IV is present, but their amplitudes, and presumably fusion pore sizes, do not vary (8). The divergence between results with amperometry and capacitance may reflect different forms of vesicles and fusion pores detected by the two techniques. Combining the two measurements with patch-amperometry may shed some light on this issue (31).

A change in conductance is likely to reflect a change in the molecular composition of the fusion pore. Based on experiments showing that mutations in the membrane anchor of syntaxin alter flux through fusion pores, a structural model for the fusion pore was proposed in which the transmembrane domains of the SNARE proteins form the walls of the pore (28,32,33). Within the framework of this model, changes in the number of SNARE complexes that come together to form a pore offer a plausible explanation for changes in pore conductance.

The luminal area of a barrel structure formed by the membrane anchors of n membrane spanning α-helical segments (Fig. 9) can be expressed as

$$A = nh^2\left(\cot\left(\frac{\pi}{n}\right) + \frac{\pi}{n} - \frac{\pi}{2}\right), \tag{3}$$

where n is the number of SNARE complexes and h is the radius of an α-helix (0.35 nm). $n = 8$ gives a pore area of 1.21 nm^2, which is very close to the average pore area of 1.20 nm^2 estimated from the control cell fusion pore conductance. $n = 10$ gives a pore area of 2.24 nm^2, which is very close to the average of 2.23 nm^2 from syt IV cells. Note that changing the number of SNARE complexes from 8 to 10 nearly doubles the fusion pore area. Thus, changing the number of SNARE complexes is a very effective way of modulating fusion pore size, as is further illustrated in a plot of fusion pore area versus n (Fig. 9 *A*). Applying the same analysis to fusion pores during full fusion gave similar results; With $n = 7$ for control cells we estimated a mean pore area of 0.76 nm^2 and with $n = 10$ for syt IV cells we estimated a mean pore area of 2.07 nm^2. It should be noted that these estimates depend on Eq. 2, which is a crude approximation and likely underestimates the true pore radius (20).

SNARE complexes form higher order aggregates in vitro and such aggregates are likely to function during exocytosis (34). Experiments in cracked PC12 cells with the cytoplasmic domain of synaptobrevin suggested that at least three SNARE complexes work together to trigger fusion (35), but estimates of this number vary and range as high as 15 (34). Our analysis of pore conductance increases induced by syt IV are well within this range and indicate that the number of SNARE complexes that combine during fusion could be subject to biological variation. Although mammalian syt IV has no known Ca^{2+}-dependent

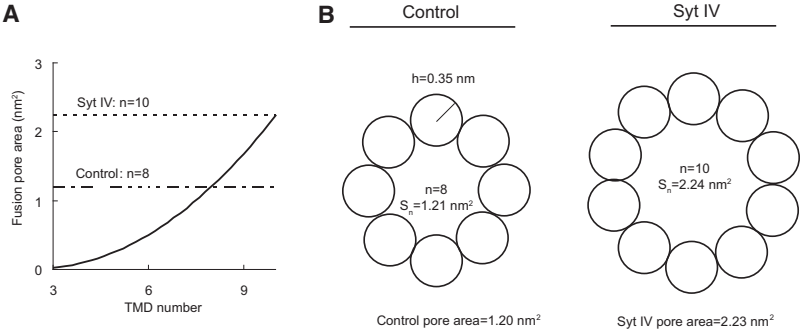

FIGURE 9 Geometry of fusion pores lined by membrane spanning helices donated by SNARE proteins. (*A*) The fusion pore area plotted versus SNARE complex number. The horizontal dotted line indicates the size of the syt IV cell DCV kiss-and-run pore. The broken line indicates the size of the control cell DCV kiss-and-run pore. (*B*) Eight syntaxin transmembrane domains form a pore with an area close to the mean area calculated for control kiss-and-run fusion pores (*left*), and 10 syntaxin transmembrane domains form a pore with an area close to the mean area calculated for syt IV cell kiss-and-run fusion pores (*right*).

interactions (2,4,8), it does bind SNARE proteins in the absence of Ca^{2+} (8) and this interaction could influence SNARE complex aggregation.

Fusion pore kinetics

These results agree with amperometry studies in PC12 cells showing that syt IV overexpression reduces exocytosis (8,9). This effect is likely a result of competition between Syt IV and the more effective Ca^{2+} sensor, syt I. Here we observed more subtle effects of Syt IV overexpression on the lifetimes of both fusion pores and endocytotic fission pores. Amperometry recording also showed that syt IV overexpression increased the duration of kiss-and-run events, although the durations of the capacitance flickers reported here (several hundred ms) were considerably longer than the stand-alone-feet seen in amperometry recording (20–80 ms) (8). This discrepancy could indicate that vesicles lacking norepinephrine account for some of our capacitance flickers. It is also possible that the minute norepinephrine fluxes in stand-alone-feet are due to fusion pores with conductances that are so low that capacitance flickers are difficult to see. However, we estimate the threshold pore conductance for detection of a 100 aF vesicle as 5 pS, and it is unlikely that the conductances of stand-alone-foot fusion pores are so low.

During full-fusion, we saw larger fusion pores with unaltered durations. During endocytosis, we saw longer duration fission pores with unaltered conductance. During kiss-and-run we saw fusion pores that were both longer in duration and larger in conductance. Previous studies of fusion pore lifetimes were interpreted with the aid of a parsimonious kinetic model (9,29).

$$\xrightarrow{k_a} C \underset{k_c}{\overset{k_o}{\rightleftarrows}} O \xrightarrow{k_d} D. \qquad \text{(Model 1)}$$

C, O, and D denote fusion pores that are respectively closed, open, and dilating. k_a is the rate constant for assembly of a closed fusion pore, k_o is the rate constant of fusion pore opening, k_c is the rate constant for closing, and k_d is the rate constant for entering a dilating state. This model predicts that the fusion pore lifetimes for kiss-and-run events, τ_{kr}, and full-fusion events, τ_{ff}, will be equal

$$\tau_{kr} = \tau_{ff} = \frac{1}{k_c + k_d}. \qquad (4)$$

Furthermore, any factor that changes fusion pore kinetics should change the lifetime of both types of event equally.

In this study, control DCV fusion pore lifetimes were significantly different between kiss-and-run and full-fusion, i.e., $\tau_{kr} \neq \tau_{ff}$. Moreover, τ_{kr} increased with syt IV overexpression, but τ_{ff} did not. These results negate Model 1 and indicate the need for modifications. Amperometry recording revealed multi-exponential fusion pore lifetime distributions that indicated the need for a kinetic model with multiple open states (8). A related model with multiple open states provides insight into these results:

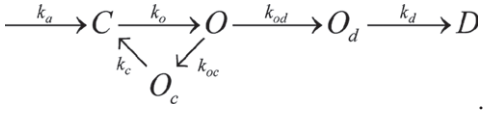

. (Model 2)

O_d denotes an open pore committed to dilation. O_c is an open state committed to closure. The rate constants are indicated for each relevant transition. Reverse rates were neglected for simplicity. This means that detailed balance will be violated but adding slow reverse rates to satisfy detailed balance should not alter the qualitative conclusions.

Model 2 has the advantage of greater robustness in allowing for differences between τ_{kr} and τ_{ff} and also allowing a factor to modulate their lifetimes independently. Model 2 specifies the mean kiss-and-run lifetime as

$$\tau_{kr} = \frac{1}{k_{od} + k_{oc}} + \frac{1}{k_c}, \qquad (5)$$

and the mean full-fusion pore lifetime as

$$\tau_{ff} = \frac{1}{k_{od} + k_{oc}} + \frac{1}{k_d}. \qquad (6)$$

We can account for the result that control DCV fusion pores had longer lifetimes for full-fusion events than for kiss-and-run events by making k_d smaller than k_c. Going from state O_c to C (with a mean time of $1/k_c$) is essentially a process of pore closure and vesicle recovery, and may conceivably also be relevant to fission pore closure. Syt IV may interact with a factor involved in pore closure, and slow the process without affecting k_d or k_{oc}. In this way the lifetimes of full-fusion events would remain unchanged even as kiss-and-run pores and fission pores are prolonged.

Endocytosis

It is notable that in addition to effects on exocytosis, syt IV overexpression also altered endocytosis. Thus, we saw that syt IV reduced the size of downward capacitance steps and increased the mean lifetime of fission pores. In peptidergic nerve terminals syt IV increased the amplitude of a slow component of endocytosis (5). The endocytosis protein dynamin has been implicated in the modulation of fusion pores (36,37). The endocytosis protein AP-2 interacts with syt I (38). Syt I has been proposed to trigger clathrin mediated endocytosis (39), and its inactivation slows endocytosis (40). Similar interactions with syt IV could underlie the dual effects on fusion and fission pores. Indeed, vesicle proteins mediating exocytosis are natural targets in molecular recognition events for endocytosis, and provide a means for selective recovery of former vesicle membrane. In this way molecules involved in exocytosis could function in endocytosis. The increasing number of ways in which syt IV modulates membrane fusion and fission suggests that it has multiple binding partners

among proteins with a variety of functions in membrane trafficking.

This work was supported by the National Institutes of Health (grant NS44057).

REFERENCES

1. Fukuda, M., T. Kojima, and K. Mikoshiba. 1996. Phospholipid composition dependence of Ca^{2+}-dependent phospholipid binding to the C2A domain of synaptotagmin IV. *J. Biol. Chem.* 271:8430–8434.
2. von Poser, C., K. Ichtchenko, …, T. C. Südhof. 1997. The evolutionary pressure to inactivate. A subclass of synaptotagmins with an amino acid substitution that abolishes Ca^{2+} binding. *J. Biol. Chem.* 272:14314–14319.
3. Wang, P., C. T. Wang, …, E. R. Chapman. 2003. Mutations in the effector binding loops in the C2A and C2B domains of synaptotagmin I disrupt exocytosis in a nonadditive manner. *J. Biol. Chem.* 278:47030–47037.
4. Dai, H., O. H. Shin, …, J. Rizo. 2004. Structural basis for the evolutionary inactivation of Ca^{2+} binding to synaptotagmin 4. *Nat. Struct. Mol. Biol.* 11:844–849.
5. Zhang, Z., A. Bhalla, …, M. B. Jackson. 2009. Synaptotagmin IV: a multifunctional regulator of peptidergic nerve terminals. *Nat. Neurosci.* 12:163–171.
6. Pawlu, C., A. DiAntonio, and M. Heckmann. 2004. Postfusional control of quantal current shape. *Neuron.* 42:607–618.
7. Dean, C., H. Liu, …, E. R. Chapman. 2009. Synaptotagmin-IV modulates synaptic function and long-term potentiation by regulating BDNF release. *Nat. Neurosci.* 12:767–776.
8. Wang, C. T., J. C. Lu, …, M. B. Jackson. 2003. Different domains of synaptotagmin control the choice between kiss-and-run and full fusion. *Nature.* 424:943–947.
9. Wang, C.-T., R. Grishanin, …, M. B. Jackson. 2001. Synaptotagmin modulation of fusion pore kinetics in regulated exocytosis of dense-core vesicles. *Science.* 294:1111–1115.
10. Clements, J. D. 1996. Transmitter timecourse in the synaptic cleft: its role in central synaptic function. *Trends Neurosci.* 19:163–171.
11. Jackson, M. B. 2007. In search of the fusion pore of exocytosis. *Biophys. Chem.* 126:201–208.
12. Stiles, J. R., D. Van Helden, …, M. M. Salpeter. 1996. Miniature endplate current rise times less than 100 microseconds from improved dual recordings can be modeled with passive acetylcholine diffusion from a synaptic vesicle. *Proc. Natl. Acad. Sci. USA.* 93:5747–5752.
13. Fulop, T., S. Radabaugh, and C. Smith. 2005. Activity-dependent differential transmitter release in mouse adrenal chromaffin cells. *J. Neurosci.* 25:7324–7332.
14. Tucker, W. C., J. M. Edwardson, …, E. R. Chapman. 2003. Identification of synaptotagmin effectors via acute inhibition of secretion from cracked PC12 cells. *J. Cell Biol.* 162:199–209.
15. Hay, J. C., and T. F. J. Martin. 1992. Resolution of regulated secretion into sequential MgATP-dependent and calcium-dependent stages mediated by distinct cytosolic proteins. *J. Cell Biol.* 119:139–151.
16. Debus, K., and M. Lindau. 2000. Resolution of patch capacitance recordings and of fusion pore conductances in small vesicles. *Biophys. J.* 78:2983–2997.
17. Klyachko, V., Z. Zhang, and M. B. Jackson. 2007. Low-noise recording of single vesicle capacitance steps in cell-attached membrane patches. *In* Methods in Molecular Biology: Exocytosis and Endocytosis Methods and Protocols. A. I. Ivanov, editor. Humana Press, Totowa, NJ.
18. Lindau, M. 1991. Time-resolved capacitance measurements: monitoring exocytosis in single cells. *Q. Rev. Biophys.* 24:75–101.
19. Lollike, K., N. Borregaard, and M. Lindau. 1995. The exocytotic fusion pore of small granules has a conductance similar to an ion channel. *J. Cell Biol.* 129:99–104.
20. Jackson, M. B. 2006. Molecular and Cellular Biophysics. Cambridge University Press, Cambridge.
21. Bauerfeind, R., A. Régnier-Vigouroux, …, W. B. Huttner. 1993. Selective storage of acetylcholine, but not catecholamines, in neuroendocrine synaptic-like microvesicles of early endosomal origin. *Neuron.* 11: 105–121.
22. Gentet, L. J., G. J. Stuart, and J. D. Clements. 2000. Direct measurement of specific membrane capacitance in neurons. *Biophys. J.* 79:314–320.
23. Neher, E., and A. Marty. 1982. Discrete changes of cell membrane capacitance observed under conditions of enhanced secretion in bovine adrenal chromaffin cells. *Proc. Natl. Acad. Sci. USA.* 79:6712–6716.
24. Fernandez, J. M., E. Neher, and B. D. Gomperts. 1984. Capacitance measurements reveal stepwise fusion events in degranulating mast cells. *Nature.* 312:453–455.
25. Klyachko, V. A., and M. B. Jackson. 2002. Capacitance steps and fusion pores of small and large-dense-core vesicles in nerve terminals. *Nature.* 418:89–92.
26. He, L., X.-S. Wu, …, L. G. Wu. 2006. Two modes of fusion pore opening revealed by cell-attached recordings at a synapse. *Nature.* 444:102–105.
27. Chizmadzhev, Y. A., P. I. Kuzmin, …, F. S. Cohen. 2000. Dynamics of fusion pores connecting membranes of different tensions. *Biophys. J.* 78:2241–2256.
28. Jackson, M. B., and E. R. Chapman. 2008. The fusion pores of Ca(2+)-triggered exocytosis. *Nat. Struct. Mol. Biol.* 15:684–689.
29. Wang, C. T., J. Bai, …, M. B. Jackson. 2006. Synaptotagmin-Ca^{2+} triggers two sequential steps in regulated exocytosis in rat PC12 cells: fusion pore opening and fusion pore dilation. *J. Physiol.* 570:295–307.
30. Eaton, B. A., M. Haugwitz, …, H. P. Moore. 2000. Biogenesis of regulated exocytotic carriers in neuroendocrine cells. *J. Neurosci.* 20:7334–7344.
31. Albillos, A., G. Dernick, …, M. Lindau. 1997. The exocytotic event in chromaffin cells revealed by patch amperometry. *Nature.* 389:509–512.
32. Han, X., and M. B. Jackson. 2005. Electrostatic interactions between the syntaxin membrane anchor and neurotransmitter passing through the fusion pore. *Biophys. J.* 88:L20–L22.
33. Han, X., C. T. Wang, …, M. B. Jackson. 2004. Transmembrane segments of syntaxin line the fusion pore of Ca^{2+}-triggered exocytosis. *Science.* 304:289–292.
34. Montecucco, C., G. Schiavo, and S. Pantano. 2005. SNARE complexes and neuroexocytosis: how many, how close? *Trends Biochem. Sci.* 30:367–372.
35. Hua, Y., and R. H. Scheller. 2001. Three SNARE complexes cooperate to mediate membrane fusion. *Proc. Natl. Acad. Sci. USA.* 98:8065–8070.
36. Jaiswal, J. K., V. M. Rivera, and S. M. Simon. 2009. Exocytosis of post-Golgi vesicles is regulated by components of the endocytic machinery. *Cell.* 137:1308–1319.
37. Tsuboi, T., H. T. McMahon, and G. A. Rutter. 2004. Mechanisms of dense core vesicle recapture following ''kiss and run'' (''cavicapture'') exocytosis in insulin-secreting cells. *J. Biol. Chem.* 279:47115–47124.
38. Grass, I., S. Thiel, …, V. Haucke. 2004. Recognition of a basic AP-2 binding motif within the C2B domain of synaptotagmin is dependent on multimerization. *J. Biol. Chem.* 279:54872–54880.
39. Takei, K., and V. Haucke. 2001. Clathrin-mediated endocytosis: membrane factors pull the trigger. *Trends Cell Biol.* 11:385–391.
40. Poskanzer, K. E., K. W. Marek, …, G. W. Davis. 2003. Synaptotagmin I is necessary for compensatory synaptic vesicle endocytosis in vivo. *Nature.* 426:559–563.